

# Particle Acceleration and gamma-ray emission due to magnetic reconnection around the core region of radio galaxies

B. Khiali<sup>1</sup>, E. M. de Gouveia Dal Pino<sup>1</sup>, and H. Sol<sup>2</sup>

<sup>1</sup> IAG-Universidade de São Paulo, Rua do Matão 1226, São Paulo, SP, Brazil  
e-mail: bkhiali@usp.br

<sup>2</sup> LUTH, Observatoire de Paris, CNRS, Universite Paris Diderot, 5 Place Jules Janssen, 92190 Meudon, France

Received September ??, 2015; accepted ??? ??, ????

## ABSTRACT

**Context.** The current detectors of gamma-ray emission specially at TeV energies have too poor resolution to determine whether this emission is produced in the jet or in the core, particularly of low luminous, non-blazar AGNs (like radio galaxies). In recent works it has been found that the power released by events of turbulent fast magnetic reconnection in the core region of these sources is more than sufficient to reproduce the observed gamma-ray luminosities. Besides, 3D MHD simulations with test particles have demonstrated that a first-order Fermi process within reconnection sites with embedded turbulence results very efficient particle acceleration rates.

**Aims.** We computed here the spectral energy distribution (SED) from radio to gamma-rays of the radio galaxies for which energy emission up to TeVs has been detected (namely, M87, Cen A, Per A, and IC 310).

**Methods.** For this aim, we employed the acceleration model above and considered all the relevant leptonic and hadronic loss processes around the core region of the sources.

**Results.** We found that the calculated SEDs match very well specially with the VHE observations, therefore strengthening the conclusions above in favour of a core emission origin for the VHE emission of these sources. The model also naturally explains the observed very fast variability of the VHE emission.

**Conclusions.**

**Key words.** Magnetic reconnection – particle acceleration – radiation mechanisms: non-thermal

## 1. Introduction

The non-thermal multi wavelength emission from active galactic nuclei (AGNs) has been broadly studied. Regarding the very high energy (VHE) emission, until recently only AGNs with highly beamed jets towards the line of sight, namely blazars, were detected by gamma-ray telescopes. More than a chance coincidence, these detections are consistent with the conventional scenario that attributes the VHE emission of these sources to particle acceleration along the jet being strongly Doppler boosted and producing apparently very high fluxes.

Lately, however, a few non-blazar sources which belong to the branch of low luminosity AGNs (or simply LLAGNs) for having bolometric luminosities of only a few times the Eddington luminosity,  $L_{Edd}$  (Ho et al. 1997; Nagar et al. 2005) have been also detected at TeV energies by ground based  $\gamma$ -ray observatories (e.g., Sol et al. 2013 and references therein). The angular resolution and sensitivity of these detectors are still so poor that it is hard to establish exactly the location of the emission, i.e. whether it comes from the jet or the core (e.g., Kachelriess et al. 2010).

Among these sources, the radio galaxies M87, Centaurus A (Cen A or NGC 5128), Persus A (Per A or NGC 1275) and IC 310 are probably the most striking cases. These VHE detections were surprising because, besides being highly underluminous, the viewing angle of the jets

of these sources is of several degrees, therefore allowing for only moderate Doppler boosting. These characteristics make it difficult explaining the VHE of these sources adopting the same standard scenario of blazars.

Furthermore, observations by *MAGIC*, *HESS* and *VERITAS* of short time scale variability in the  $\gamma$ -ray emission of IC 310, M87 and Per A (Aharonian et al. 2006; Abdo et al. 2009a; Ackermann et al. 2012; Aleksić et al. 2010a,b, 2012a,b, 2014a,c) indicate that it is produced in a very compact region that might be the core. In the case of Cen A, though there is no evidence of significant variability at  $E > 100$  MeV, GeV or TeV bands by *Fermi-LAT* (Abdo et al. 2010) or *HESS* (Aharonian et al. 2009), it has been also argued that the *HESS* data of this source would be more compatible with a point source near the core (Kachelriess et al. 2010). If the  $\gamma$ -ray photons were due, for instance, to proton-proton ( $pp$ ) interactions along the jet then on leaving the source they would interact with the extragalactic background light (EBL) resulting in a flatter spectrum in the TeV range which is not compatible with *HESS* measurements (Kachelriess et al. 2009b, see however, other potential explanations in §. 5).

Though a number of works have attempted to explain these observations as produced in the large scale jets of these sources (e.g., Stawarz et al. 2006), the evidences above led to the search for alternative particle acceleration scenarios involving the production of the VHE in the sur-

rounds of the nuclear black hole (BH), for instance, in a pulsar-like cascade mechanism in the BH magnetosphere (e.g., Neronov & Aharonian 2007), or in the sub-parsec scale jet (e.g., Tavecchio & Ghisellini 2008; Abdo et al. 2009b). In particular, Tavecchio & Ghisellini (2008), invoked a two zone model with a jet with a fast spine and a slower layer to explain the TeV flares, while Lenain et al. (2008) proposed that the emission would occur while the jet is collimating, and Georganopoulos et al. (2005) while it is decelerating. Another process to explain these VHE flares has been proposed by Giannios et al. (2010) in which misaligned mini-jets driven by magnetic reconnection are moving within the jet with relativistic velocities relative to it. A two-step acceleration model to TeV energies was also proposed by Istomin & Sol (2009) in the surrounds of the BH involving initial particle acceleration within the accretion disk and then further centrifugal acceleration in the rotating magnetosphere.

In this work, we consider an alternative model in which particles are accelerated, through a first-order Fermi process, in the surrounds of the BH by the magnetic power extracted from fast magnetic reconnection events occurring between the magnetosphere of the BH and the magnetic field lines arising from the inner accretion disk (see Figure 1). Inspired by similar phenomena occurring in space environments, like the earth magnetotail and the solar corona, de Gouveia Dal Pino & Lazarian (2005) explored this process first in the framework of microquasars and then de Gouveia Dal Pino et al. (2010a) and de Gouveia Dal Pino et al. (2010b) extended it to AGNs.

In these works, de Gouveia Dal Pino & Lazarian (2005) and de Gouveia Dal Pino et al. (2010a) found that fast reconnection could be efficient enough to produce the core radio outbursts in microquasars and AGNs. More recently, Kadowaki et al. (2015) (henceforth KGS15) and Singh et al. (2015) revisited this model exploring different mechanisms of fast magnetic reconnection and accretion, and extending the study to include also the gamma-ray emission of a much larger sample containing more than 230 sources. They confirmed the earlier trend found by de Gouveia Dal Pino & Lazarian (2005) and de Gouveia Dal Pino et al. (2010a), and verified that if fast reconnection is driven by turbulence (Lazarian & Vishniac 1999) there is a correlation between the fast magnetic reconnection power and the BH mass spanning  $10^{10}$  orders of magnitude that can explain not only the observed radio, but also the VHE luminosity from microquasars and LLAGNs (involving all the sources of the so called fundamental plane of BH activity Merloni et al. 2003).

The correlations found in the works above (specially in KGS15 and Singh et al. 2015) between the calculated power released by magnetic reconnection in the surrounds of the BH and the observed radio and gamma-ray luminosities of a very large sample of LLAGNs and microquasars, have motivated further investigation to test the validity of the model. In particular, in a recent work, we explored in detail the non-thermal emission of the microquasars Cygnus X-1 and Cygnus X-3 and found that this reconnection acceleration model is able to reproduce most of the features of their observed spectral energy distribution (SED) in outburst states up to TeV energies (Khiali et al. 2015 hereafter KGV15).

Our aim here is to extend this study to the supermassive BH sources of the KGS15 and Singh et al. (2015) sample,

trying to reconstruct the observed SEDs, specially at the VHE branch, of the four radio galaxies mentioned earlier, i.e., Centaurus A, Per A, M87 and IC 310 applying the same acceleration model above.

We first compute the power released by fast magnetic reconnection in the surrounds of the BH as described, and then the resulting particle spectrum of the accelerated particles in the magnetic reconnection site. In particular, we explore the first-order Fermi acceleration process that may occur within the current sheet as proposed in de Gouveia Dal Pino & Lazarian (2005). Such acceleration mechanism has been extensively tested numerically in 3D collisional MHD simulations of magnetic current sheets employing test particles (Kowal et al. 2011, 2012; de Gouveia Dal Pino et al. 2014) and also in collisionless particle in cell simulations (e.g., Drake et al. 2006; Zenitani et al. 2009; Drake et al. 2010; Cerutti et al. 2013, 2014; see also the reviews by de Gouveia Dal Pino et al. 2014; de Gouveia Dal Pino & Kowal 2015).

In order to reconstruct the SED, we consider the relevant radiative processes due to the interactions of the accelerated particles by magnetic reconnection with the surrounding radiation, matter and magnetic fields. We then compare the rates of these radiative losses with the magnetic reconnection acceleration rate and determine the maximum energy that the electrons and protons can attain. For comparison, we also consider the acceleration rate due to shocks in the surrounds of the reconnection region, but find that this is less effective than the acceleration by magnetic reconnection.

We show for the first time that a consistent and numerically tested acceleration model by magnetic reconnection in the surrounds of BH sources can effectively reproduce the observed SEDs of the four radio galaxies up to TeVs.

The outline of the paper is as follows. In Section 2, we describe in detail our scenario presenting both the acceleration model and the emission mechanisms. In section 3, we show the results of the application of the acceleration and emission model to Cen A, Per A, M87 and IC 310. Finally, we discuss and summarize our results drawing our conclusions in Section 4.

## 2. Description of the acceleration and emission model

As stressed, we consider here that relativistic particles may be accelerated in the core of LLAGNs, i.e., in the coronal region around the BH near the basis of the jet launching, as a result of events of fast magnetic reconnection and examine whether this process may reproduce the observed emission specially at VHEs. This model has been described in detail by de Gouveia Dal Pino & Lazarian (2005) and de Gouveia Dal Pino et al. (2010a), and more recently by KGS15. We summarize below its main characteristics. We assume that the inner region of the accretion disk/corona system alternates between two states which are controlled by changes in the global magnetic field. Right before a fast magnetic reconnection event, we adopt the simplest possible configuration by considering a magnetized standard geometrically thin and optically thick accretion disk around the BH as in the sketch of Figure 1 (see also Singh et al. 2015 for an alternative solution considering a magnetic-ADAF accretion disk).

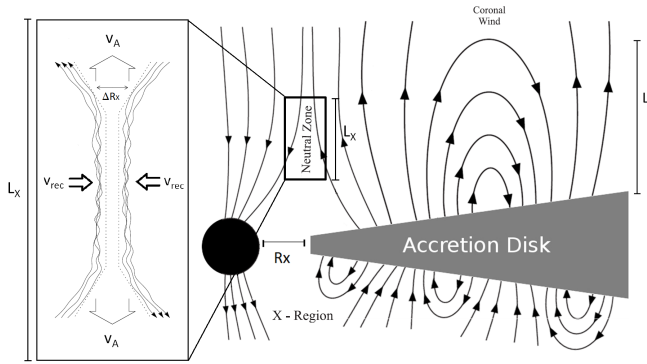


**Fig. 1.** Scheme of magnetic reconnection between the lines rising from the accretion disk into the corona and the lines around the BH horizon. Reconnection is made fast by the presence of embedded turbulence in the reconnection zone (as indicated in the detail). Particle acceleration may occur in the magnetic reconnection zone by a first-order Fermi process (adapted from de Gouveia Dal Pino & Lazarian 2005).

The magnetosphere around the central BH can be built from the drag of magnetic field lines by the accretion disk (e.g., MacDonald et al. 1986; Koide et al. 2002). The large-scale poloidal magnetic field in the disk corona can in turn be formed by the action of a dynamo inside the accretion disk or dragged from the surroundings. Under the action of disk differential rotation, this poloidal magnetic flux gives rise to a wind that partially removes angular momentum from the system and increases the accretion rate. This, in turn, increases the ram pressure of the accreting material that will press the magnetic lines in the inner disk region against the lines of the BH magnetosphere thus favouring the occurrence of reconnection (see Figure 1). We note that according to mean field dynamo theory, an inversion of the polarization of the magnetic lines is expected to occur every half of the dynamo cycle; when this happens a new flux of disk lines should reach the inner region with an inverted polarity with respect to the magnetic flux already sitting around the BH, therefore, favouring magnetic reconnection between the two fluxes. The advection of field lines from the outer regions also allows for periodic changes in the polarity. Also for simplicity, we assume the co-rotation between the inner disk region and the BH magnetosphere.

The magnetic field intensity in this inner region can be determined from the balance between the magnetic pressure of the BH magnetosphere and the accretion ram pressure and is given by (KGL15):

$$B \cong 9.96 \times 10^8 r_X^{-1.25} \xi^{0.5} m^{-0.5} \text{ G}, \quad (1)$$

where  $m$  is the BH mass in units of solar mass,  $\xi$  is the mass accretion disk rate in units of the Eddington rate ( $\xi = \dot{M}/\dot{M}_{Edd}$ , with  $\dot{M}_{Edd} = 1.45 \times 10^{18} m \text{ g s}^{-1}$ ), and  $r_X = R_X/R_S$  is the inner radius of the accretion disk in units of the BH Schwarzschild radius ( $R_S = \frac{2GM}{c^2}$ ). As KGS15, we adopt here  $r_X = 6$ .

### 2.1. Conditions for fast reconnection in the surrounds of the BH

As discussed in KGS15, the presence of embedded turbulence in the nearly collisional MHD coronal flow of the core

region of the AGNs can make reconnection very fast (e.g., Lazarian & Vishniac 1999) and cause the release of large amounts of magnetic energy power in the scenario described in Figure 1.<sup>1</sup>

According to the model proposed by Lazarian & Vishniac (1999), even weak embedded turbulence causes the wandering of the magnetic field lines which allows for many independent patches to reconnect simultaneously making the global reconnection rate large,  $V_R \sim v_A (l_{inj}/L)^{1/2} (v_{turb}/v_A)^2$ , where  $V_R$  is the reconnection speed,  $v_A$  is the Alfvén speed, and  $l_{inj}$  and  $v_{turb}$  the injection scale and velocity of the turbulence, respectively. This expression indicates that the reconnection rate can be as large as  $\sim V_A$ .

This theory has been deeply investigated (e.g. Eyink et al. 2011; Lazarian et al. 2012) and confirmed numerically (Kowal et al. 2009, 2012). In particular, it has been shown (Eyink et al. 2011) that turbulent collisional fast reconnection prevails when the thickness of the magnetic discontinuity layer (see Eq. 3 below, and Figure 1) is larger than the ion Larmor radius. As demonstrated in KGS15, for the systems we are studying this condition is naturally satisfied and we will adopt this process to derive the magnetic power released by fast reconnection. We should also notice that there has been direct evidences of turbulent reconnection in solar coronal events (e.g., Priest 2001) and also in the Earth magnetotail (Retinò et al. 2007).

The fluids we are investigating here have large hydrodynamical and magnetic Reynolds numbers (KGS15) implying that they can be easily distorted and become turbulent. For instance, current driven instabilities, can naturally drive turbulence with characteristic velocities around the particles thermal speed. Also, the occurrence of continuous slow magnetic reconnection during the building of the corona itself in the surrounds of the BH (Liu et al. 2003) will contribute to the onset of turbulence which will then be further fed by fast reconnection as in the Lazarian & Vishniac (1999) model (see Oishi et al. 2015; Lazarian et al. 2015). Numerical simulations of coronal disk accretion also indicate the formation of turbulent flow in the surrounds of the BH (see e.g, Dexter et al. 2014). All these processes may ensure the presence of embedded weak turbulence in the magnetic discontinuity described in Figure 1.<sup>2</sup>

The magnetic reconnection power released by turbulent driven fast reconnection in the magnetic discontinuity region (as schemed in Figure 1), has been derived in KGS15

<sup>1</sup> We note that the strongly magnetized and low dense coronal fluid of the systems we are considering in this work satisfies the condition  $L > l_{mfp} > r_l$  (where  $L$  is a typical large scale dimension of the system,  $l_{mfp}$  the ion mean free path and  $r_l$  the ion Larmor radius). For such flows a weakly collisional or effectively collisional MHD description is more than appropriate and we will employ this approach here (see more details in KGS15).

<sup>2</sup> We note that in the model described here, the turbulence is in general sub-Alfvénic due to the strong magnetic fields implied and nearly trans-sonic (since the turbulent velocity is of the order of the sound speed and smaller than the Alfvén speed) and therefore, incompressible. This regime of turbulence has been extensively investigated in the literature (see e.g., Lazarian & Vishniac 1999; Lazarian et al. 2012) and the acceleration formulae employed here have been obtained directly from numerical MHD simulations with particle tests injected in current sheets with embedded turbulence also implying this regime (Kowal, de Gouveia Dal Pino, Lazarian 2012).

and is given by:

$$W \simeq 1.66 \times 10^{35} \psi^{-0.5} r_X^{-0.62} l^{-0.25} l_X q^{-2} \xi^{0.75} m \text{ erg s}^{-1}, \quad (2)$$

where  $l = L/R_S$  is the height of the corona in units of  $R_S$ ;  $l_X = L_X/R_S$ ,  $L_X \leq L$  is the extension of the magnetic reconnection zone (as shown in Figure 1; see also Table 1),  $q = [1 - (3/r_X)^{0.5}]^{0.25}$  and  $v_A = v_{A0}\psi$  is the relativistic form of the Alfvén velocity, with  $v_{A0} = B/(4\pi\rho)^{1/2}$ ,  $B$  being the local magnetic field,  $\rho \simeq n_c m_p$  the fluid density in the corona,  $n_c$  the coronal number density,  $m_p$  the proton mass, and  $\psi = [1 + (v_{A0}/c)^2]^{-1/2}$ , in this work,  $v_{A0} \sim c$ . The results of KGS15 (Figure 5 in KGS15) have shown that accretion rates  $\xi$  between  $0.05 < \xi \leq 1$  are able to produce magnetic reconnection power values which are larger than the observed luminosities of LLAGNs. We adopt here  $\xi \simeq 0.7$ , but we should notice that the results are not very much sensitive to the choice of this parameter. As demonstrated in KGS15 and SKG15 studies, one can match the observations by taking alternative fiducial combinations of the free parameters in the equation above, particularly by constraining the size of the height of the corona,  $L$ .

We will employ the equations above in Section 3 to model the acceleration of particles in the core of Cen A, Per A, M87 and IC 310. The acceleration region in our model corresponds to the cylindrical shell around the BH where magnetic reconnection takes place (see Figure 1). This shell has a length  $l_X$ , with inner and outer radii given by  $R_X$  and  $R_X + \Delta R_X$  respectively, where  $\Delta R_X$  is the width of the current sheet given by (KGS15):

$$\Delta R_X \simeq 2.34 \times 10^4 \psi^{-0.31} r_X^{0.48} l^{-0.15} l_X q^{-0.75} \xi^{-0.15} m \text{ cm}. \quad (3)$$

In §. 3, we will also need the accretion disk temperature in order to evaluate the black body radiation field:

$$T_d \simeq 3.71 \times 10^7 \alpha^{-0.25} r_X^{-0.37} m^{0.25} \text{ K}, \quad (4)$$

where  $0.05 \leq \alpha < 1$  is the Shakura-Sunyaev disk viscosity parameter which we here assume to be of the order of 0.5.

In addition, we will need the coronal number density to compute the radiative losses of accelerated particles which is (KGS15)

$$n_c \simeq 8.02 \times 10^{18} r_X^{-0.375} \psi^{0.5} l^{-0.75} q^{-2} \xi^{0.25} m^{-1} \text{ cm}^{-3}, \quad (5)$$

while the coronal temperature is given by

$$T_c \simeq 2.73 \times 10^9 r_X^{-0.187} \psi^{0.25} l^{0.125} q^{-1} \xi^{0.125} \text{ K}. \quad (6)$$

The magnetic power in Eq. 2 heats the surrounding gas and accelerates particles. As in KGV15, we assume that approximately 50% of the reconnection power is used to accelerate the particles. This is consistent with plasma laboratory experiments of particle acceleration in reconnection sheets (e.g., Yamada et al. 2014) and also with the observations of flares in the Sun (e.g., Lin & Hudson 1971).

## 2.2. Particle acceleration due to magnetic energy released by fast reconnection

A first-order Fermi acceleration may occur when particles of the fluid are trapped between the two converging magnetic flux tubes moving to each other in the magnetic reconnection discontinuity with a velocity  $V_R$ . de Gouveia

Dal Pino & Lazarian (2005) first investigated this process analytically and showed that, as the particles bounce back and forth undergoing head-on collisions with magnetic fluctuations in the current sheet, their energy increases by  $< \Delta E/E > \sim 8V_R/3c$  after each round trip, which leads to an exponential energy growth after several round trips. If magnetic reconnection is fast,  $V_R$  is of the order of the local Alfvén speed  $V_A$  and, at the surroundings of relativistic sources  $V_R \simeq v_A \simeq c$  and thus the mechanism can be rather efficient.

From the results of 3D MHD numerical simulations of this process (Kowal et al. 2012), we find that the acceleration rate for a proton is given by (KGV15):

$$t_{acc,rec,p}^{-1} = 1.3 \times 10^5 \left( \frac{E}{E_0} \right)^{-0.4} t_0^{-1}, \quad (7)$$

where  $E$  is the energy of the accelerated proton,  $E_0 = m_p c^2$ ,  $m_p$  is the proton rest mass,  $t_0 = l_{acc}/v_A$  is the Alfvén time, and  $l_{acc}$  is the length scale of the acceleration region.

Similarly, for the electrons one can get:

$$t_{acc,rec,e}^{-1} = 1.3 \times 10^5 \sqrt{\frac{m_p}{m_e}} \left( \frac{E}{E_0} \right)^{-0.4} t_0^{-1}, \quad (8)$$

where  $m_e$  is the electron rest mass.

The two equations above do not take into account the effects of radiative losses upon the accelerated particles. They will be used to compute the acceleration rates in our model.

As stressed in de Gouveia Dal Pino & Lazarian (2005), it is also possible that a diffusive shock may develop in the surrounds of the magnetic reconnection zone at the jet launching region caused by plasmons or coronal mass ejections. As in solar flares, these can be produced in the reconnection layer and released along the magnetic field lines. In this case, we expect the shock velocity to be predominantly parallel to the magnetic lines. and the acceleration rate for a particle of energy  $E$  will be approximately given by (e.g., Spruit 1988):

$$t_{acc,shock}^{-1} = \frac{\eta e c B}{E}, \quad (9)$$

where  $0 < \eta \ll 1$  characterizes the efficiency of the acceleration. We fix  $\eta = 10^{-1}$ , which is appropriate for shocks with velocity  $v_s \approx 0.1c$  commonly assumed in the Bohm regime.

In §. 3 we compare both the magnetic reconnection acceleration time (Eqs. 7 & 8) and the shock acceleration time (Eq. 9) with the relevant radiative cooling process that cause the loss of energy of the accelerated particles and constrain their maximum energy. These particles may lose energy via interactions with the surrounding magnetic field (producing synchrotron emission), the photon field (producing inverse Compton, synchrotron-self-Compton, and photo-meson interactions), and with the surrounding matter (producing pp collisions and relativistic Bremsstrahlung radiation). In §. 2.4, we discuss the relevant radiative loss processes for electrons and protons which will allow the construction of the SED of the sources M87, Cen A, Per A and IC 310 for comparison with the observations.

### 2.3. Particle energy distribution

The accelerated particles are expected to develop a power law spectrum. Their injection and cooling will occur mainly in the coronal region around the black hole (see Figure 1). The isotropic injection function (in units of  $\text{erg}^{-1}\text{cm}^{-3}\text{s}^{-1}$ ) is given by (see e.g. KGV15):

$$Q(E) = Q_0 E^{-p} \exp[-E/E_{max}] \quad (10)$$

with  $p > 0$  and  $E_{max}$  the cut-off energy which can be calculated by the balance of acceleration and the energy losses. Particles can gain energy up to a certain value  $E_{max}$  for which the total cooling rate equals the acceleration rate.

We assume for the power law index  $p$  values between 1 and 2.5 for the sources here investigated (see §. 3), which are compatible with the analytical and numerical studies of particle acceleration within magnetic reconnection sheets (e.g., Drury 2012; Kowal et al. 2012).

The normalization constant  $Q_0$  is calculated from the total power injected in each type of particle

$$L_{(e,p)} = \int_V d^3r \int_{E_{min}}^{E_{max}} dE E Q_{(e,p)}(E) \quad (11)$$

where  $V$  is the emission volume in the surrounds of the magnetic reconnection acceleration region in Figure 1 (see §. 2.5) and  $L_{(e,p)}$  is the fraction of the magnetic reconnection power that accelerates the electrons and protons calculated from Eq. 2. This injected power is equally shared between protons and electrons.

The kinetic equation that describes the general evolution of the particle energy distribution  $N(E, t)$  is the Fokker-Planck differential equation (Ginzburg & Syrovatskii 1995). We here use a simplified form of this equation. We employ the one-zone approximation to find the particle distribution, assuming that the acceleration region is spatially thin enough, so that we can ignore spatial derivatives in the transport equation. Physically, this means that we are neglecting the contributions to  $N(E)$  coming from other regions than the magnetic reconnection region in the inner accretion disk/corona zone in the surrounds of the BH. We consider a steady-state particle distribution which can be obtained by setting  $\frac{\partial N}{\partial t} = 0$  in the Fokker-Planck differential equation, so that the particle distribution equation is

$$N(E) = \left| \frac{dE}{dt} \right|^{-1} \int_E^\infty Q(E) dE. \quad (12)$$

Here  $-\frac{dE}{dt} \equiv Et_{cool}^{-1}$ , where  $t_{cool}^{-1}$  is the total cooling rate that can be calculated assuming all the cooling mechanisms (we describe them in the following section briefly).

### 2.4. Photon Absorption

We consider two main absorption processes of the photons produced by the accelerated particles in the nuclear region of the sources: the gamma-ray photon absorption due to  $e^-e^+$  pair creation, and the absorption of optical and X-ray photons due to external interstellar neutral gas and dust (photon-neutral) absorption.

#### 2.4.1. Photon-photon ( $\gamma\gamma$ ) annihilation

The produced  $\gamma$ -rays can be annihilated by the surrounding radiation field via electron-positron pair production, i.e.,  $\gamma + \gamma \rightarrow e^+ + e^-$ . In our model the dominant radiation field for this process in the coronal region is due to the scattered photons from the accretion disk (see Figure 2).<sup>3</sup>

To evaluate the optical depth due to this process, we have adopted the model described in Cerutti et al. (2011), assuming that the  $\gamma$ -rays are produced within a spherical region around the disk with radius extending up to  $L \simeq 20R_S$ . The attenuated  $\gamma$ -ray luminosity  $L_\gamma(E_\gamma)$  at a distance  $z$  above the disk is given by (Romero & Christiansen 2005)

$$L_\gamma(E_\gamma) = L_\gamma^0(E_\gamma) e^{-\tau(z, E_\gamma)} \quad (13)$$

where  $L_\gamma^0$  is the intrinsic coronal gamma-ray luminosity and  $\tau(z, E_\gamma)$  is the optical depth. The calculated optical depth depends on the  $\gamma$ -ray energy and the distance above the disk  $z$ .

Figure 2 depicts the gamma-ray absorption spectrum for the sources investigated here, for different heights  $z$ . We see that in all cases at distances larger than  $\sim 0.1R_S$  from the disk surface, the absorption of  $\gamma$ -rays becomes negligible. Since we are adopting here an emission region with an extension  $\simeq 0.3R_S$  to  $\simeq 20R_S$ , it is reasonable to exclude the absorption effect above in our calculations of the SEDs (see §. 3).

#### 2.4.2. Photon-neutral ( $\gamma N$ ) interactions

The low energy photons produced in the nuclear emission region will propagate in the surrounding interstellar medium of the host galaxy filled mainly by hydrogen and helium gas. Photons with energies larger than the hydrogen Lyman threshold (13.6 eV) will be able to photo-ionize the neutral gas.

The optical depth resulting from these interactions is approximately given by

$$\tau_{\gamma H}(E_\gamma) = N_H \sigma_{\gamma N}(E_\gamma) \quad (14)$$

where  $N_H$  is the neutral hydrogen column density, and  $\sigma_{\gamma N}$  is the absorption cross section. As in Reynoso et al. 2011, we take this from Ryter (1996) for  $E_\gamma < 1$  keV considering that atomic hydrogen and galactic dust are the dominant components of the environment. The values of  $N_H$  for each source investigated here are taken from the observations and are listed in Table 1.

This  $\gamma N$  absorption has been considered in the reconstruction of the SEDs of the four LLAGNs in §. 3. As we will see there, the photons produced in the optical-soft X-ray range are fully absorbed by these interactions.

### 2.5. Radiative cooling processes

In this section we discuss briefly the relevant radiative loss processes for electrons and protons.

We take into account both leptonic and hadronic radiative loss mechanisms in the emission region. This corresponds to the torus with volume  $V$  that encompasses the

<sup>3</sup> We should remark that we found the contribution due to the coronal radiation field itself to be much smaller than that of the accretion disk.

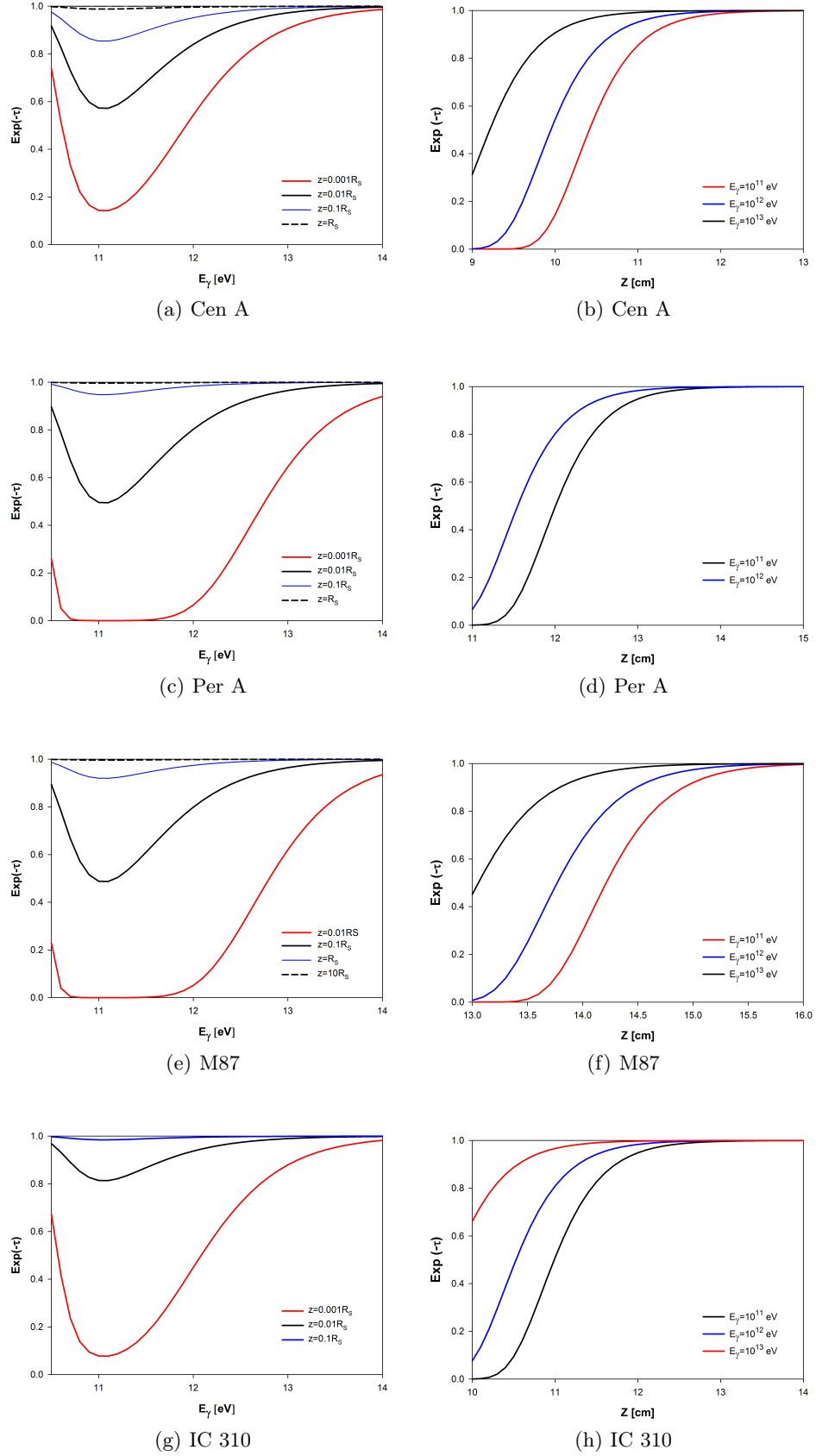


**Fig. 2.** Left panels: Spectrum of  $\gamma$ -ray absorption at selected heights  $z$  above the plane of the disk in Cen A, Per A, M87, and IC 310 (a, c, e, and g panels, respectively). Right panels: The transmitted flux  $\exp(-\tau)$  for different  $\gamma$ -ray energies as function of the height  $z$  above the disk in Cen A, Per A, M87, and IC 310 (b, d, f, and h panels, respectively).

**Table 1.** Model parameters for Cen A, Per A, M87 and IC 310.

	Parameters	Cen A	Per A	M 87	IC 310
$B$	Magnetic field (G)	$1.25 \times 10^4$	4812	1620	8874
$W$	Magnetic reconnection power (erg/s)	$1.2 \times 10^{43}$	$8.2 \times 10^{43}$	$5.25 \times 10^{44}$	$4.5 \times 10^{43}$
$\Delta R_X$	Width of the current sheet (cm)	$3.6 \times 10^{13}$	$2.4 \times 10^{14}$	$1.35 \times 10^{15}$	$3.2 \times 10^{12}$
$n_c$	Coronal particle number density ( $\text{cm}^{-3}$ )	$7.1 \times 10^9$	$10^9$	$3.3 \times 10^8$	$10^{11}$
$T_d$	Temperature of the disk (K)	$1.9 \times 10^8$	$3 \times 10^8$	$5.2 \times 10^8$	$2.25 \times 10^8$
$R_x$	Inner radius of disk (cm)	$8.8 \times 10^{13}$	$6 \times 10^{14}$	$5.3 \times 10^{15}$	$1.7 \times 10^{14}$
$L_X$	Extension of the reconnection region (cm)	$1.5 \times 10^{14}$	$10^{15}$	$4.4 \times 10^{15}$	$8.8 \times 10^{12}$
$L$	Extension of the corona (cm)	$3 \times 10^{14}$	$2 \times 10^{15}$	$4.4 \times 10^{15}$	$8.8 \times 10^{12}$
$V$	Volume of emission region ( $\text{cm}^3$ )	$7.8 \times 10^{43}$	$2.3 \times 10^{46}$	$10^{48}$	$1.36 \times 10^{41}$
$d$	Distance of the source(Mpc)	3.8	75	16.7	78
$m$	Mass of BH ( $M_\odot$ )	$5 \times 10^7$	$3.4 \times 10^8$	$3 \times 10^9$	$10^8$
$p$	Injection spectral index	2.4	2.15	2.4	1.7
$\gamma_{min}$	Particle minimum Lorentz factor	6	2	4	2
$N_H^*$	Dust/neutral gas column density ( $\text{cm}^{-2}$ )	$10^{23}$	$4 \times 10^{20}$	$2 \times 10^{20}$	$1.2 \times 10^{21}$

\* The observed values for  $N_H$  of Cen A, Per A, M87 and IC310 are taken from

Morganti et al. (2008); Canning et al. (2010); Lieu et al. (1996) and Kalberla et al. (2010), respectively.

cylindrical shell where magnetic reconnection particle acceleration takes place in Figure 1. Considering that the cylinder extends up to  $L$  in both hemispheres, then the small radius of the torus is  $r = L/2$  and the large radius is  $R_X$ , so that the effective emission zone in our model has an approximate volume  $V = \pi^2 L^2 R_X$ .

For leptonic processes, we consider the interactions of relativistic electrons with the surrounding magnetic, charged matter, and photon fields.

Accelerated electrons spiralling in the magnetic field emit synchrotron radiation. We calculate the synchrotron loss rate for the sources considered here and the radiated synchrotron spectrum as functions of the scattered photon energy (see Eqs. 10 and 11 in KGV15). Electron interactions with the electrostatic field of nuclei of charge  $Ze$  allow for the production of bremsstrahlung radiation. Finally, relativistic electron interactions with photons may produce inverse Compton (IC) radiation. We considered different photon fields in the surrounds of BH, namely, the scattered photons from accretion disk and core black-body radiation (Eq. 36 in KGV15) and the electron synchrotron emission (which allows for SSC; Eq. 14 in KGV15) and found that the latter, i.e., the SSC mechanism is dominant in the inner coronal/accretion disk region we are interested in this work.

Accelerated protons produce hadronic emission from interactions with the magnetic field (synchrotron), and also through the decay of neutral pions. These are produced either by inelastic collisions with nuclei of the corona ( $pp$  interactions; Eqs. 19 & 21 of KGV15), or via interactions with photons, in photo-meson production ( $p\gamma$  mechanism; Eqs. 40 & 43 in KGV15). The latter mechanism takes place for photon energies greater than  $E_{th} \approx 145$  MeV in the reference frame of the relativistic proton. A single pion can be produced in an interaction near the threshold and then decay giving rise to gamma-rays. In our model the dominating photon field comes from the synchrotron radiation.

4

<sup>4</sup> We find that for photo-meson production, the radiation from the accretion disk and from the corona are irrelevant compared to the contribution from the synchrotron emission.

The cooling rates due to these leptonic and hadronic mechanisms are plotted as functions of the particle energy for the sources here studied in Figures 3a, 5a, 7a and 9a, and Figures 3b, 5b, 7b and 9b, respectively, where they are also compared with the acceleration rates due to shock and magnetic reconnection.

The radiative losses considered above are used to calculate the SEDs of the sources in §3.

### 3. application to radio galaxies

We describe here the results of the application of the model described above to Cen A, Per A, M87 and IC 310 which are classified as radio galaxies. As remarked in §. 1, these radio galaxies have been observed at VHE by *FERMI-LAT*, *VERITAS* and *HESS* (e. g., Abdo et al. 2009c, 2010; Abramowski et al. 2012; Aleksić et al. 2014b).

In general lines, in all cases, the procedure to calculate the SED begins with the determination of the total power released by fast magnetic reconnection within the acceleration region (Eq. 2), that is, in the cylindrical shell of height  $L_X$  and thickness  $\Delta R_X$  (Eq. 3) (see Figure 1). This power is then employed to compute the spectrum of accelerated electrons and protons (Eq. 12) that will be injected into the emission volume  $V$ , i.e., the torus that surrounds the acceleration region (as described in §. 2.5). The parameters employed for each source are given in Table 1. We note that our model has actually only 7 free parameters (i.e.,  $R_x$ ,  $L_X$ ,  $L \leq L$ ,  $p$ ,  $\gamma_{min}$ ,  $\xi$  and  $\alpha$ ). The remaining quantities of Table 1 are obtained directly from these parameters through Eqs. 1 to 5 (i.e.,  $B$ ,  $W$ ,  $\Delta R_X$ ,  $n_c$  and  $T_d$ ), or from the observations (i.e.,  $d$  and  $m$ ). The maximum energy that each particle spectrum can attain is obtained from the comparison of the acceleration rates, for both electrons and protons, with the relevant radiative loss processes (seen §. 2). As remarked, the accelerated electrons will loose energy by synchrotron, IC and Bremsstrahlung mechanisms, with a dominance of the synchrotron process shaping their spectrum. The fluxes of these emission processes are then calculated and also the number density of the synchrotron photons that are partially self-scattered by the electrons (leading to SSC emission) and by protons (in  $p\gamma$  interactions). Likewise, the energy distribution of the protons is



also calculated taking into account the radiative cooling mechanisms due to synchrotron,  $pp$  and  $p\gamma$  interactions (see §2.3) that will shape the very high energy part of the SED.

### 3.1. Application to Cen A

The Prominent radio galaxy Cen A (or NGC 5128) is the nearest FR I active radio galaxy to Earth ( $z=0.0018$ , Graham 1978), at a distance of  $\simeq 3.8$  Mpc (Rejkuba 2004), making it uniquely observable among this class of objects and an excellent source for studying the physics of relativistic outflows as well as of the core region. Cen A is one of the best well known extragalactic objects over a wide range of frequencies and the photon emission from the nuclear region of the galaxy has been detected from the radio to the  $\gamma$ -rays band. Cen A has been proposed as a possible source of UHE cosmic rays (with energies  $\leq 6 \times 10^{19}$  eV; Abraham et al. 2007) by the Pierre Auger collaboration. The SMBH mass inferred from kinematics of stars, as well as  $H_2$  and ionized gas is estimated to be in the range of  $\sim 10^7 - 10^8 M_\odot$  (Marconi et al. 2006; Neumayer et al. 2007), and here we adopted the value  $5 \times 10^7 M_\odot$ . The viewing angle of the jet ( $\theta$ ) is still debatable, for instance at parsec scales it is  $\theta \sim 50^\circ - 80^\circ$  (Tingay et al. 1995), whereas at the 100 pc scale  $\theta \sim 15^\circ$  (Hardcastle et al. 2003).

In this section we show the results for Cen A obtained by applying the model described in §. 2 around the nuclear region, employing the set of parameters listed in Table 1.

The values for the first five parameters in Table 1 have been calculated from Eqs. 1-4 and 5. We take for the accretion disk inner radius the value  $R_X = 6R_S$ , for the extension  $L_X$  of the reconnection region (see Figure 1), we consider the value  $L_X \simeq 10R_S$ , and for the extension of the corona  $L \simeq 20R_S$ . As remarked earlier, the volume  $V$  of the emission region in Table 1 was calculated by considering the torus that encompasses the reconnection region in Figure 1. The magnetic reconnection power  $W$  is evaluated from Eq. 2.

Figure 3 shows the radiative cooling rates for the different energy loss processes for electrons and protons as described in Section 2.4. These are compared with the acceleration rates due to first-order Fermi acceleration both within the magnetic reconnection site (Eqs. 7 & 8) and behind a shock (Eq. 9). We notice that at high energies for both protons and electrons the acceleration is dominated by the first-order Fermi magnetic reconnection process in the core region. Besides, the main radiative cooling process for the electrons is synchrotron radiation (Figure 3a), while for protons the photo-meson production ( $p\gamma$  interactions) governs the loss mechanisms (Figure 3b). For the  $p\gamma$  interactions, we have found that the proper target radiation field is that of the photons from the electron synchrotron emission.

The intercept between the magnetic reconnection acceleration rate and the synchrotron rate in Figure 3a gives the maximum energy that the electrons can attain in this acceleration process, which is  $\sim 3 \times 10^{11}$  eV. Protons on the other hand, do not cool as efficiently as the electrons and can attain energies as high as  $\sim 2.5 \times 10^{17}$  eV.

We have constructed the SED of Cen A using a lepton-hadronic model where particles are accelerated close to the central BH by magnetic reconnection and interact with the surrounding fields radiating in a spherical region of radius

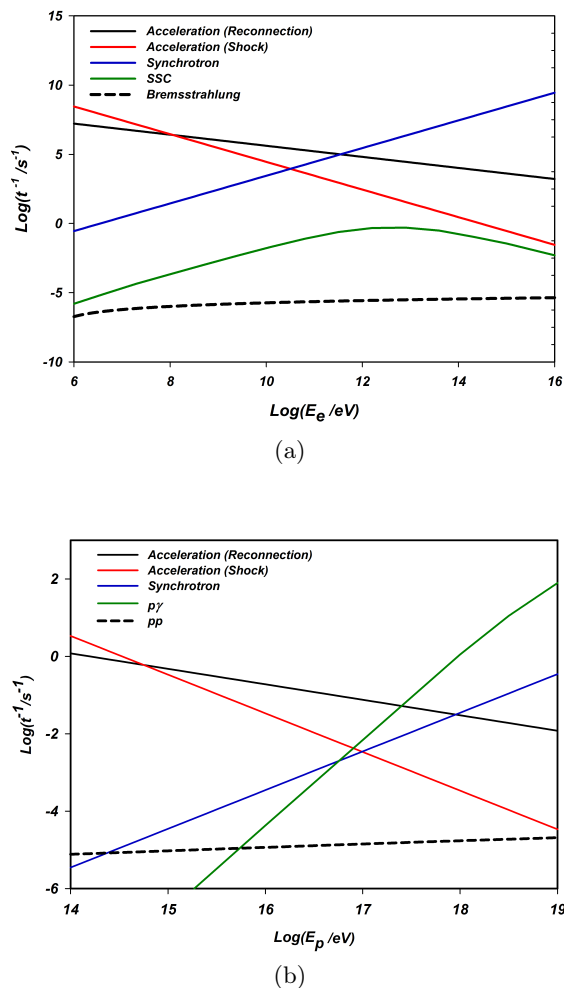


**Fig. 3.** Acceleration and cooling rates for electrons (a) and protons (b) in the nuclear region of Cen A.

$L$  (see section 2.4). The SED is depicted in (Figure 4) where it is compared with the observations.

We note that the data presented in this figure in the low and intermediate energy ranges come mostly from archival data and represent typical average emission and activity. The emission in the high energy range obtained by *Fermi-LAT* and *HESS* at the same epoch correspond to non-variable and moderate activity too.

As described in section 2.3, we have adopted a particle energy injection power law function:

$$Q(E) \propto E^{-p}. \quad (15)$$

In Figure 4, we considered injected primary particles with  $p = 2.4$  which is consistent with theoretical predictions of particle acceleration within magnetic reconnection sites (see §. 2.3). Our calculations show that synchrotron radiation explains the observed emission in the radio to visible band, while SSC is the dominant mechanism to produce the observed hard X-rays and low energy  $\gamma$ -rays as a result of interactions between energetic electrons with scattered synchrotron photons. Also in the Figure, neutral pion ( $\pi^0$ ) decays can explain the observed  $\gamma$ -rays at TeV energies, via  $pp$  and  $p\gamma$  interactions which are the two main processes producing  $\pi^0$ .



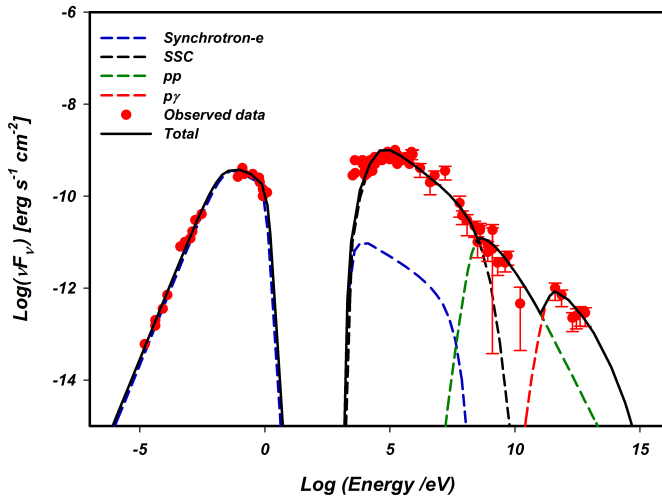


**Fig. 4.** Calculated spectral energy distribution (SED) for Cen A using the magnetic reconnection acceleration model in a lepton-hadronic scenario compared with observations. The data depicted in the radio to optical energy range ( $10^{-5}$  eV – 1 eV) is from SCUBA at  $800 \mu\text{m}$  (Hawarden et al. 1993), ISO & SCUBA at  $450 \mu\text{m}$  and  $850 \mu\text{m}$  (Mirabel et al. 1999); the data in the hard x-rays range is from *Swift-BAT* (Ajello et al. 2009) and *Suzaku* (Markowitz et al. 2006). We also include data from *OSSE* (Kinzer et al. 1995) and *COMPTEL* (Steinle et al. 1998) in the range of  $5 \times 10^5 - 10^7$  eV. The data observed in the energies  $10^8 - 10^{10}$  eV are taken by *EGRET* (Sreekumar et al. 1999; Hartman et al. 1999) and in the energies  $10^8 - 10^{10}$  eV by *Fermi-LAT* (Abdo et al. 2009b, 2010). The TeV data are taken by *HESS* (Aharonian et al. 2009).

We note that in order to fit the observed data in the radio to optical range, we had to assume a minimum energy for the injected electrons in the acceleration zone (Eq. 11 in KGV15),  $E_{\min} = (\gamma_{\min} - 1)m_e c^2$ , with  $\gamma_{\min} = 6$ . Though this injected value has no influence on the VHE tail of the SED, it is determinant in the match of the low energy branch. We have found that values of  $\gamma_{\min} < 6$  do not lead to the synchrotron match in the low energy range (see also §4).

As remarked in §. 2.4, the  $\gamma$ -ray absorption due to pair production occurs according to Figures 2a and 2b very near the accretion disk at heights smaller than  $\sim 0.001 R_S$ , thus much smaller than the emission region that extends up to  $\sim 20 R_S$  in our model, so that  $\exp(-\tau) \simeq 1$  and the absorption effect is not effective at the heights of interest. On the other hand, due to the high dust and neutral gas column density in Cen A ( $N_H = 10^{23} \text{cm}^{-2}$ , see e.g., Morganti et al. 2008) we find that the optical to soft X-ray emission is fully absorbed via  $\gamma N$  absorption (see figure 4, Eq. 14).

### 3.2. Application to Per A

Perseus A (also known as NGC 1275 and 3C 84), is a nearby active galaxy located at the centre of the Perseus cluster and hosts a central SMBH mass of  $\sim 3.4 \times 10^8 M_\odot$  (Wilman et al. 1994). In fact, Per A is one of the closest  $\gamma$ -ray emitting AGNs. Its distance to the Earth is 75 Mpc (Brown & Adams 2011) and is also of great interest, specially due to its proximity, also providing an excellent opportunity to study the physics of relativistic outflows. Per A also seems to ex-

hibit jet precession with an orientation angle  $\approx 30^\circ - 55^\circ$  (Walker et al. 1994; see also Falceta-Gonçalves et al. 2010), which may be an indication that Per A is the result of a merger between two galaxies (Liu and Chen 2007). It is a very bright radio galaxy showing an extended jet with FR I morphology (e.g., Vermeulen et al. 1994; Buttiglione et al. 2010) with asymmetric jets at both kpc (Pedlar et al. 1990) and pc scales (Asada et al. 2006).

The parameters of our model for producing the SED of Per A are tabulated in Table 1. The first five parameters are calculated from Eqs. 1- 4 and 5. As for Cen A, we have also used for the accretion disk inner radius the value  $R_X = 6 R_S$  and for the extension  $L_X$  of the reconnection region the values  $L_X = 10 R_S$  and  $L \simeq 20 R_S$ .

The radiative loss and acceleration rates for electrons and protons are compared in Figure 5. As in Cen A, magnetic reconnection is the dominant acceleration mechanism over shock acceleration at the high energy branch for both electrons and protons and determines the maximum energy that the particles can achieve before losing part of it radiatively. Electrons may be accelerated up to  $3 \times 10^{11}$  eV and the main process to cool them is synchrotron. While the maximum energy the protons can achieve is  $10^{17}$  eV and *photo-meson* production ( $p\gamma$ ) is the dominant mechanism to cool them. Similarly to Cen A, the dominant photon field interacting with the accelerated protons is the synchrotron radiation.

We have constructed the SED for this source employing a leptonic scenario (Figure 6). In this case, the primary particles were injected with a power law spectral index  $p = 2.15$  (Eq. 10). The radio spectrum is matched by electron synchrotron emission, with particles injected into the acceleration zone with rest mass energy (i.e., with  $\gamma_{\min} = 2$ ). The observed X-ray and  $\gamma$ -ray emission is nearly reproduced by SSC occurring in the nuclear region in a spherical region of radius  $L \sim 20 R_S$ , as described in §. 2.4. However, it should be noticed that there is a high intensity BATSE data point in the  $\sim 10^5$  eV that is not matched by the model. Given the fact that this source is highly variable, this feature probably corresponds to a more active state superposed to the less active one (represented by the less intense data points in the same energy range).

The observations also indicate that there is a high energy cut-off around  $\sim 3 \times 10^{11}$  eV in this source. In our scenario this is due to leptonic emission produced by interactions of high energy electrons with the radiation field produced by themselves and this cut-off is compatible with the maximum energy calculated from the comparison of the reconnection acceleration rate with the synchrotron loss rate in Fig. 5a.

As stressed in §. 2.5, the optical depth for the produced  $\gamma$ -rays was also calculated in this case and is shown in Figures 2c and 2d). We note that the 100 GeV  $\gamma$ -rays may be fully absorbed due to pair production but only very near to disk ( $z < 0.001 R_S$ ). However, these vertical distances from the disk, comparing to the length scale of the emission region is very small and reasonably, we can ignore the absorption effect at the heights larger than  $\sim R_s$  which is compatible with extension of emission region in our model.

Similarly to Cen A, the neutral gas and dust of the interstellar medium of the host galaxy in this source also causes the extinction of the emission in the range of  $10 - 10^2$  eV (Fig. 6; see also §. 2.4.2).

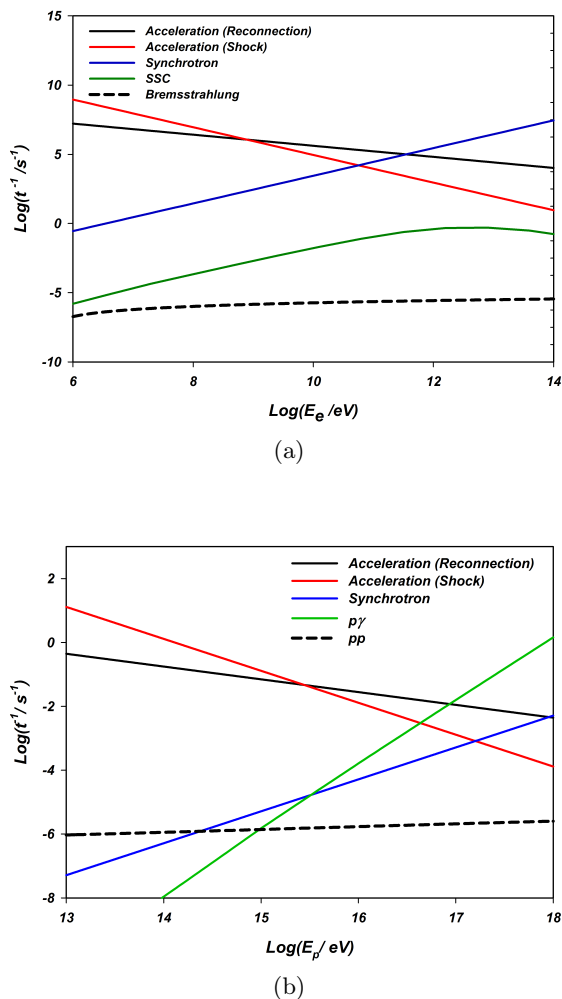


**Fig. 5.** Acceleration and cooling rates for electrons (a) and for protons (b) in the nuclear region of Per A (NGC 1275).

### 3.3. Application to M87

The FR I giant radiogalaxy M87 is another well-known nearby AGN located at 16.7 Mpc within the Virgo cluster which harbours a SMBH with a mass of  $M_{BH} \sim 6 \times 10^9 M_\odot$  (e. g., Gebhardt & Thomas 2009) which, along with Cen A and Per A, has been known as a peculiar extragalactic laboratory to study high energy astrophysics and investigate the nonthermal mechanisms of VHE emission in AGNs. The observations indicate that its jet is oriented within  $20^\circ$  of the line of sight (Biretta et al. 1999), so that as in the other cases, no significant Doppler boosting is expected for the  $\gamma$ -ray flux.

The TeV  $\gamma$ -ray signal from M87 was first reported by *HEGRA* (Aharonian et al. 2003) and then confirmed by *HESS* (Aharonian et al. 2006). The latter also revealed that this emission is strongly variable with time scales of 1-2 days and thus produced in a very compact region, as pointed out before.

Table 1 shows the parameters that we used to calculate the acceleration and cooling rates and also to reconstruct the SED of this source.

In Figures 7, we compare the rates of the radiative cooling processes with the rates of the acceleration mechanisms

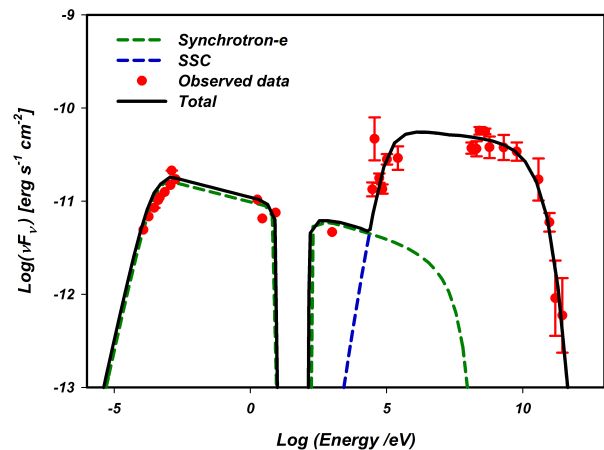


**Fig. 6.** A leptonic model to reproduce the SED of Per A (NGC 1275) using the magnetic reconnection acceleration model. Data include *MOJAVE* (Lister et al. 2009), *Planck* (Ade et al. 2011), HST (Chiaberge et al. 1999), and HST FOS (Johnstone & Fabian 1995) for the radio to optical spectrum; data depicted in X-rays is from the XMM (Torres 2012), *Swift*-BAT (Ajello et al. 2009), and BATSE (Harmon et al. 2004); and data depicted in the gamma-ray band is from *Fermi*-LAT (Abdo et al. 2009a; Ackermann et al. 2012) in the 100 MeV-100GeV energy range, and from *MAGIC* (Aleksić et al. 2010a,b, 2012a,b) in the VHE tail. We note that the error bars for the BATSE data (in the  $10^5$  eV range) were evaluated using Harmon et al. (2004); Soldi et al. (2014) and Wilson et al. (2012).

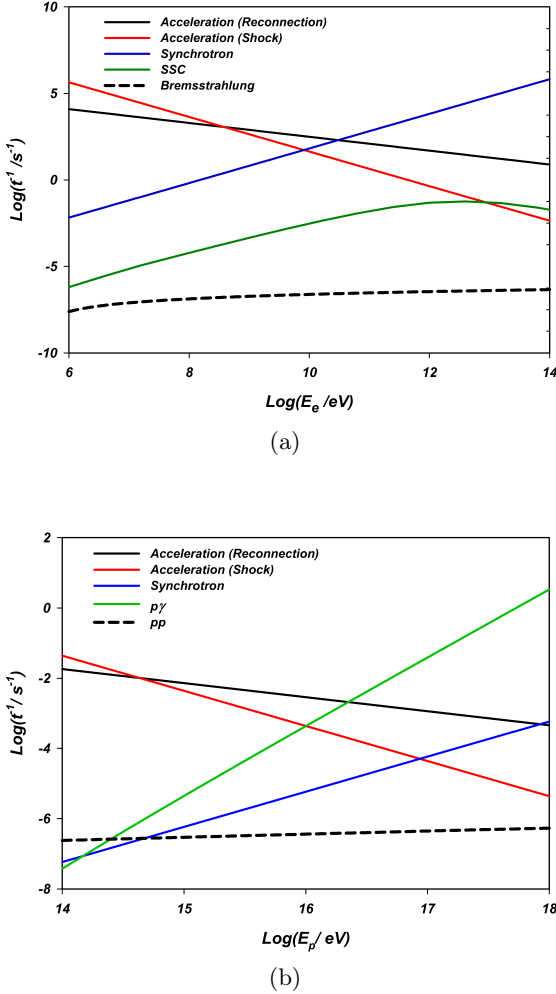
for electrons and protons. As in the other two sources, we find that the dominant energy loss mechanisms are the synchrotron and the  $p\gamma$  interactions for electrons and protons, respectively, and the acceleration is dominated by the magnetic reconnection process which defines the energy cut off for both electrons and protons. Figure 7a indicates that this maximum energy is  $\sim 4 \times 10^{10}$  eV for electrons and  $\sim 5 \times 10^{16}$  eV for protons.

Figure 8 shows the calculated SED for M87 compared to the observations. It is also reproduced by a lepton-hadronic model in the core region as described in §. 2, where we assumed an injected particle energy distribution  $\propto E^{-p}$  with a power index  $p = 2.4$ .

With an electron minimum energy  $E_{min} = 4m_e c^2$ , we can fit the observed core radio to visible spectrum by synchrotron emission.

As in Cen A, the low and intermediate energy data in Figure 8 from archive and represent typical average emission. The data obtained by *Fermi*-LAT ( $10^8 - 10^{11}$  eV) and by *HESS* (the TeV tail) correspond both to more quiescent states and have been taken in different epochs. They are reproduced in our model by different mechanisms. While *Fermi*-LAT data are fitted by SSC and  $pp$  collisions, *HESS* data are fitted by the decay of neutral pions from  $p\gamma$  interactions with photons coming from the synchrotron radiation. We note that an observed flare state by *HESS* (Aharonian et al. 2006; not shown in Fig. 8) can be also reproduced by our model assuming a flatter injection particle spectrum with a spectral index  $= 2.1$ .

Figures 2e and 2f show the absorbed  $\gamma$ -ray flux for M87. As in the other cases, this absorption is significant only at heights smaller than  $R_S$  and therefore, its effect can



**Fig. 7.** Acceleration and cooling rates for electrons (a) and for protons (b) in the nuclear region of M87.

be neglected at the much larger emission scales considered here.

The absorption of low energy photons by interstellar neutral gas and dust in this source is also important (Fig. 8).

We note that our model and the chosen parametrization is also consistent with the observed TeV rapid variability of M87 which is  $\sim 1 - 2$  days (Abramowski et al. 2012) implying an extremely compact emission region (corresponding to scales of only a few  $R_S$ ). As remarked in §2.4, the emission region in our model corresponds to the torus region that encompasses the cylindrical shell where magnetic reconnection particle acceleration takes place in Figure 1, i.e., the effective emission zone in our model has a thickness  $\simeq L$ . For this source  $L \simeq 5R_S$  (see Table 1), which is of the order of the inferred scale from the observed variability.

### 3.4. Application to IC 310

The peculiar galaxy IC 310 (also named B0313+411 and J0316+4119 in observational reports) is one of the brightest objects which, as Per A, is also located in the Perseus galaxy cluster at a distance of 78 Mpc from Earth (Aleksić et al. 2014c) and harbours a supermassive BH with a mass of

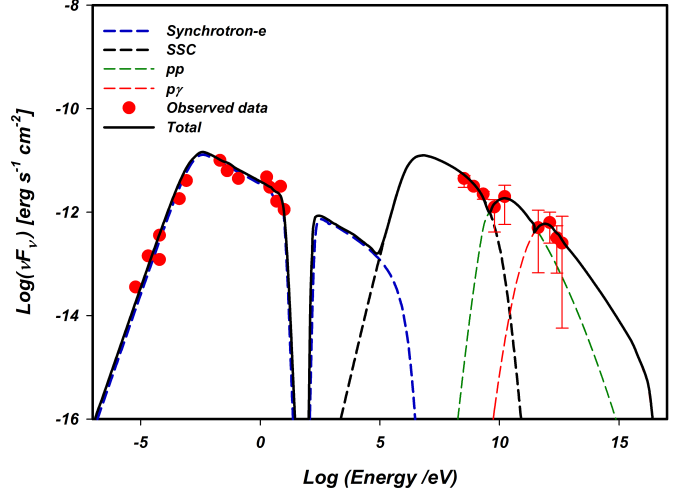


**Fig. 8.** A lepton-hadronic model of the SED of M 87 compared with observations. The core radio data are obtained from MOJAVE VLBA (Kellermann et al. 2004) at 15 GHz, from (Biretta et al. 1991) at 1.5, 5 and 15 GHz, from IRAM (Despringre et al. 1996) at 89 GHz, from SMA at 230 GHz (Tan et al. 2008), from Spitzer at 21 and 7.2 GHz (Shi et al. 2007) and from Gemini (Perlman et al. 2001) at 3.2 GHz. Optical-UV emission from HST (Sparks et al. 1996). MeV/GeV  $\gamma$ -ray data are from *Fermi-LAT* (Abdo et al. 2009c), and the low-state TeV spectrum (Aharonian et al. 2006) from *HESS*.

$\sim 10^8 M_\odot$  (Aleksić et al. 2014c). The redshift of this source is  $z=0.0189$  (Bernardi et al. 2002) which has made it the fourth nearest AGN at VHE gamma-rays (Kadler et al. 2012), after Cen A with  $z=0.00183$ , M 87 with  $z=0.004$  and Per A with  $z=0.017559$ .

IC 310 has been observed at energies  $E > 100$  GeV by MAGIC (Mariotti et al. 2010) and Fermi-LAT collaboration also reported the detection of photons above 30 GeV (Neronov et al. 2010). However the origin of the gamma-ray emission is not clear yet and both the jet and the core have been considered as possible emission regions.

Recently, MAGIC collaboration has reported fast time variability for IC 310 on the VHE  $\gamma$ -ray with time scales  $\sim 4.8$  min (Aleksić et al. 2014a,c) which constrains the size of the emission zone to 20% of its  $R_S$ .

The parameters we used to calculate the acceleration and cooling time scales and also to reconstruct the SED of this source are shown in Table 1.

The comparison between the acceleration and cooling rates are depicted in Figures 9a and 9b for electrons and protons, respectively. As in the other cases, we see that the calculated maximum energy for both electrons and protons reaches larger values for magnetic reconnection than for shock acceleration, so that magnetic reconnection should be the dominating mechanism to accelerate particles in the nuclear region of this source as well. The diagrams indicate that electrons can accelerate up to  $8 \times 10^{10}$  eV, while the protons up to  $2 \times 10^{17}$  eV. Also in this source synchrotron emission is the dominant loss mechanism for electrons and  $p\gamma$  radiation is the dominant one for protons for energies larger than  $\sim 10^{15}$  eV.

Figure 10 shows the calculated SED for IC 310. As in the other sources, the observed radio emission can be explained

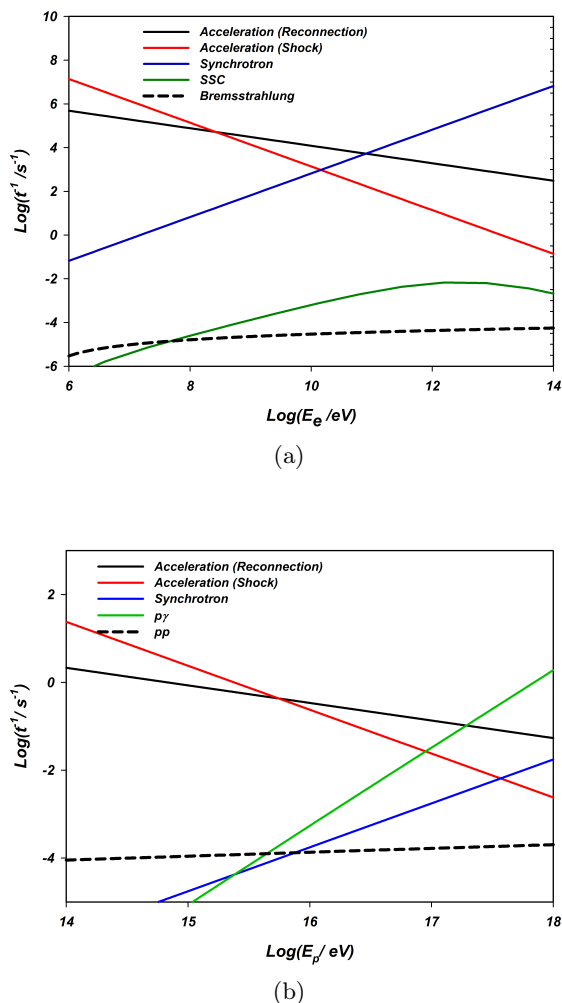


**Fig. 9.** Acceleration and cooling rates for electrons (a) and for protons (b) in the nuclear region of IC 310.

by synchrotron and the TeV  $\gamma$ -rays by the  $pp$  and  $p\gamma$  processes due to particles injected with a power law spectral index  $p=1.7$ . The core opacity to this emission has been also calculated for IC 310 in figure 2 which indicates that the  $\gamma$ -ray absorption is negligible in the emission length scales here considered which are above  $0.3R_S$ .

Also in this case the radiation in low energy range ( $10 - 10^2\text{eV}$ ) is fully absorbed due to photon-neutral interactions (Figure 10).

As for M87, our model and the adopted parametrization can also naturally explain the fast variability of the VHE  $\gamma$ -rays in 3C 310. The effective emission zone for this source is  $L \simeq 0.3R_S$  according to our model (see Table 1), which is compatible with the scale inferred from the observed high variability in the  $\gamma$ -ray emission,  $\sim 4.8$  min.

#### 4. Discussion and Conclusions

Our main purpose here was to explore an alternative mechanism to explain the spectral energy distribution (SED) and, particularly, the VHE emission in non-blazar AGNs, i.e., those for which the jet probably does not point to the line of sight and therefore, do not have their emission enhanced by Doppler boosting in the relativistic jet. Instead,

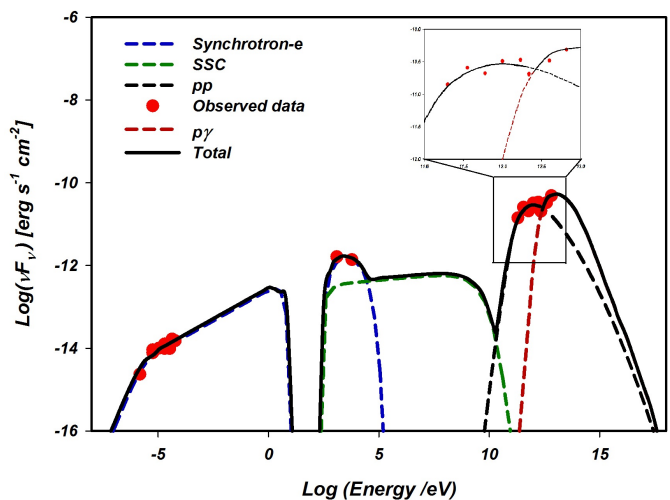


**Fig. 10.** A lepton-hadronic model of the SED of IC 310 compared with observations. The core radio data are obtained from Kadler et al. 2012; Dunn et al. 2010; Becker et al. 1991; White & Becker 1992; Condon et al. 2002; Douglas et al. 1996. The X-ray data are from XMM-Newton (Sato et al. 2005) and the VHE  $\gamma$ -ray data are from *MAGIC* (Aleksić et al. 2014c). In the upper right side of the diagram it is depicted the detail of the modeling of the VHE branch.

we have examined an acceleration mechanism occurring in the innermost region of the AGN. Based on recent results by de Gouveia Dal Pino et al. (2010a), KGS15, and Singh et al. (2015) we investigated the role of fast magnetic reconnection events in accelerating particles in the nuclear regions of low luminosity AGNs, applying this acceleration model to reconstruct the SED of Cen A, Per A, M87 and IC 310.

According to this model, trapped particles within the magnetic reconnection discontinuity formed by the encounter of the magnetic field lines arising from the accretion disk with those of the BH magnetosphere (Figure 1), can be accelerated to relativistic velocities by a first-order Fermi process in the surrounds of the BH, as described in de Gouveia Dal Pino & Lazarian (2005). Magnetic reconnection events will occur specially when there is substantial increase in the disk accretion rate which helps to press the two magnetic fluxes together. Since turbulence is expected to be present in these systems (see §. 2.1), the reconnection can be made naturally fast by it (Lazarian & Vishniac 1999 and Kowal et al. 2009).

KGS15 and Singh et al. (2015) used this model to compute the magnetic power released by reconnection in the surrounds of the BHs and compared it with the core radio and  $\gamma$ -ray luminosities of outbursts of a sample with more than 230 sources including the microquasars and LLAGNs of the fundamental plane of BH activity (Merloni et al. 2003) and also hundreds of blazars and GRBs. They have found that the reconnection power is large enough and is correlated with the observed luminosities of the microquasars and LLAGNs, following the observed trend for more than  $10^{10}$  orders of magnitude in luminosity and mass of these sources.<sup>5</sup>

<sup>5</sup> We note that this power is generally not enough to reproduce the radio or gamma-ray luminosities of the blazars and GRBs,



These correlations found with the emission of microquasars and LLAGNs are very important, because they connect the non-thermal emission, specially the VHE one, with the core of these sources, offering a reliable, self-consistent mechanism for their origin. However, in order to determine the real effectiveness of this mechanism, it is necessary to reproduce the SEDs of these sources based on this model. This has been done recently for two microquasars Cyg X1 and Cyg X3, for which the observed SEDs have been successfully reproduced by the model above (KGV15). In this work we have extended this analysis applying the reconnection model to the four radio galaxies with detection of VHE emission up to TeV.

Considering all relevant leptonic and hadronic radiative loss times due to the interactions of the accelerated particles with matter, radiation and magnetic field in the core regions of Cen A, Per A, M87 and IC 310, we compared these times with the acceleration times and found larger energy cut-offs for particles being accelerated by magnetic reconnection than by diffusive shock (see Figures 3, 5, 7, and 9). This result stresses the importance of magnetic reconnection as a potential acceleration mechanism in the core regions around BHs and compact sources in general.

Moreover, we note that the maximum energies for the electrons and protons obtained from these comparisons, are actually much smaller than the maximum possible energy that the particles can attain within the acceleration region in the reconnection sheet. The latter is constrained by the thickness of the acceleration region, i.e.,  $\Delta R_X$  (given by Eq. 3) which must be larger than or equal to the particle Larmor radius,  $r_L = E/ceB$ . This implies that the maximum energy to which the particles can be accelerated by magnetic reconnection is  $\sim 10^{20}$  eV, so that the reconnection layer is large enough to accelerate the particles to UHEs. This value reassures the efficiency of this acceleration process and suggests that if the surrounds of the BHs in AGNs were not so full of interacting matter and radiation fields they might be excellent sites for the production of UHECRs.

The cut-off values above were employed in the determination of the accelerated particle fluxes in the construction of the SED of the sources. The electron synchrotron cooling rate is found to be larger than any other loss mechanism in all leptonic energy range (Figures 3a, 5a, 7a, and 9a). Also, it is the dominant process providing the radiation field that produces the SSC and the photo-meson ( $p\gamma$ ) radiation in the SEDs of the four sources. We have also found that the  $p\gamma$  process is the dominant mechanism to cool the accelerated relativistic protons in the high energy branch. This is shown in Figure 3b for Cen A for proton energies  $\geq 6 \times 10^{16}$  eV, and in Figure 5b for Per A for proton energies  $\geq 2 \times 10^{15}$  eV, while in figures 7b and 9b for M87 and IC 310, we see that synchrotron radiation can cool the protons for energies  $\leq 2 \times 10^{15}$  eV, but for larger energies it is overcome by the  $p\gamma$  mechanism.

In summary, we have shown that, employing fiducial parameters, our acceleration model is capable of explaining the non-thermal low and high energy emission of the SED of the four investigated LLAGNs Cen A (Figure 4), Per A (Figure 6), M87 (Figure 8) and IC 310 (Figure 10).

but this is compatible with the notion that the emission in these cases is produced outside the core, at the jet that points to the line of sight and screens any deep nuclear emission.

An interesting advantage of the model presented here is the relatively small number of free parameters used to construct the SED (seven). In particular, we adopted an one-zone approximation in order to avoid the introduction of more free-parameters. Furthermore, this work is a first attempt to test the acceleration model by magnetic reconnection in the surrounds of these BH sources whose physics and distribution of the photon, density and magnetic fields are still poorly known making the use of multi-zone models even more challenging or artificial. Unlike other models (e.g. Kachelriess et al. 2009b), our acceleration mechanism was used to constrain the characteristics of the acceleration region. While most of the models take the maximum energy of the particles as a free parameter to fit the SED (e.g. Abdo et al. 2009a,b,c, 2010; Kachelriess et al. 2010), our model determines this directly from the acceleration model, as described.

#### 4.1. Cen A

According to our results for Cen A, the observed hard X-rays and *Fermi* – *LAT*  $\gamma$ -ray data can be interpreted as due to SSC and  $pp$  interactions, respectively, with accelerated particles injected in the nuclear region (at distances  $\sim 20R_S$ ) driven by magnetic reconnection with a distribution with power law index  $p = 2.4$ . The TeV radiation observed by *HESS*, on the other hand, is explained by neutral pion decays resulting from  $p\gamma$  interactions.

In Sahu et al. 2012, the authors also showed that the TeV  $\gamma$ -rays in Cen A could be explicated by  $p\gamma$  interactions, but between relativistic protons accelerated by Fermi process in shocks along the jet with the monochromatic photons observed at 170keV. Another model (Reynoso et al. 2011) also proposed particle acceleration at the jet basis with the production of the hard X-rays by synchrotron emission, and the *Fermi* – *LAT* and *HESS* data by IC and  $pp$  mechanisms, respectively, along the jet. Kachelriess et al. 2010, on the other hand, have argued against the production of the  $\gamma$  – rays in Cen A by  $pp$  interactions along the jet because on leaving the source they would interact with the EBL resulting in a flatter spectrum in the TeV range than the observed one by *HESS* (see also §. 1).

All these studies demonstrate that the origin of the VHE emission in this source is still highly debatable. A core origin, as the one suggested in this work arises as an interesting possibility as long as magnetic activity is significant in the surrounds of BHs, and it might be considered as well. To disentangle this puzzle we will need substantially improved observations, specially in the  $\gamma$ -ray range. It is possible that with the much larger resolution and sensitivity of the forthcoming CTA observatory (Actis et al. 2011; Acharya et al. 2013; Sol et al. 2013), and with longer times of exposure of this nearby source (and also of M87, Per A and IC 310), we may collect higher resolution data, and more significant information on variability that may help to determine the location of the emission region.

#### 4.2. Per A

In the case of Per A, there is no relevant data yet in TeV energies, but our core model can nearly explain the observed *Fermi* – *LAT* and *MAGIC* data in the 0.1 GeV – 650 GeV range with a leptonic scenario dominated by SSC. The

synchrotron photons that are absorbed in SSC are produced by accelerated electrons by magnetic reconnection in the coronal nuclear region around the BH (within distances  $\sim 20R_S$ ) having a distribution with a power law index  $p = 2.15$ .

An SSC model has been also proposed by Aleksić et al. (2014b), but they assumed that the Per A core could be a BL Lac blazar with the jet bending strongly at larger scales and the high energy non-thermal radiation could be originated in a sub-structure of the jet near the core pointing towards our line of sight. This bending still requires observational support and any evidence of jet precession (e.g., Walker et al. 1994; Falceta-Gonçalves et al. 2010) may favour this model. But our proposed model dismisses the necessity of such a strong bending and besides, is supported by the correlations with the observations found in KGS15 and Singh et al. (2015).

#### 4.3. M87

In the case of M87, we have applied the same magnetic reconnection model in the nuclear region around the BH (within a region of  $20 R_S$ ) considering the injection of the accelerated particles with a power law index  $p = 2.4$ . This has resulted a lepton-hadronic scenario for the SED with SSC emission and neutral pion decays from  $pp$  collisions explaining the *Fermi* – *LAT* data. We also found that the decay of the neutral pions due  $p\gamma$  interactions can explain the observed data by *HESS* in the TeV range.

The suggested sites of TeV emission for this source in former works range from large scale structures of the kpc jet (Stawarz et al. 2005) to a compact peculiar hot spot (the so-called HST-1 knot) at a distance 100 pc along the jet (Stawarz et al. 2006) and inner (sub-parsec) parts of the sources. Reynoso et al. (2011) for instance, considered that this emission is produced in the jet, but reconstructed all the emission features, which are highly variable and possibly non-simultaneous, with a single  $pp$  mechanism.

Giannios et al. (2010), on the other hand, proposed that compact minijets induced by magnetic reconnection moving relativistically within the jet in different directions, some of which pointing to our line of sight, might explain the short-time variable TeV flares observed in M87. This model bears several similarities with ours as it proposes that the minijets are generated by reconnection events in the core region, and then move out with the jet flow up to scales of  $\sim 100R_S$ . Our model also predicts the development of outbursts with the formation of reconnected features (plasmons) that may be carried out with the jet and might explain e.g., observed superluminal features near the jet basis (de Gouveia Dal Pino & Lazarian 2005, de Gouveia Dal Pino et al. 2010a). However, Giannios et al. (2010) study provides no predictions for the SED structure of M87.

In addition, there is an extensive list of models that propose that the variable VHE emission of M87 can be originated in the inner jet. These span from leptonic models, such as the decelerating flow (Georganopoulos et al. 2005), the spine-shear (Tavecchio & Ghisellini 2008), and the mini/multi-blob model (Lenain et al. 2008), to hadronic models with the emission due to proton synchrotron- $p\gamma$  interactions (Reimer et al. 2004), or  $pp$  interactions in a cloud-jet scenario (Barkov et al. 2012). However, the location of the emission region is still an unsolved problem.

Neronov & Aharonian (2007) also proposed a nuclear origin for the TeV emission of M87 coming directly from the magnetosphere of the black hole (see also Levinson 2000). They showed that accelerated electrons in the strong rotation-induced electric fields in vacuum gaps in the BH magnetosphere, similar to a pulsar magnetosphere, could lead to the observed TeV emission. Since the acceleration and emission mechanisms occurs in a very compact region close to the event horizon of the BH, it potentially can explain the observed variability of TeV  $\gamma$ -ray emission from M87. Besides, as in our model, they also explain this emission as due to  $p\gamma$  interactions with an IR compact target photon field produced by synchrotron emission. However, as stressed in §. 3, the attenuation of  $\gamma$ -ray emission due to electron-positron pair production may be significant in distances smaller than or equal to  $\sim R_S$  (Figure 2), which may affect their results. In our model, the emission scales are larger ( $\sim 5R_S$ ) making these attenuation effects negligible.

#### 4.4. IC310

In the case of IC 310, also a lepton-hadronic model in the nuclear region is able to explain the observed SED features with protons and electrons accelerated by magnetic reconnection and injected in the emission region with a power law distribution with index  $p = 1.7$ . As remarked, the observed radio emission is well fitted by synchrotron and the VHE emission detected by *MAGIC* can be explained by decays of neutral pions resulting from  $pp$  and  $p\gamma$  interactions.

Our model with an appropriate choice of parameters is also able to explain naturally the time variability detected in the sources here investigated. In particular, the very fast variability reported for the IC 310  $\gamma$ -ray emission of about  $\sim 4.8$  min (Aleksić et al. 2014c) implies an emission region scale of  $\simeq 0.3R_S$ . To explain this variability and compactness of the emission region, Aleksić et al. 2014c suggested that the particles could be accelerated by electric fields in the BH magnetosphere, as in pulsar models. Nevertheless, as demonstrated, the model described here reproduces the observed SED with an emission region with a similar size as above.

In conclusion, in the construction of the SEDs for the sources discussed here (Cen A, Per A, M87 and IC 310) based on our magnetic reconnection model in the core region, the observed emission at low energies (radio to optical) can be explained by synchrotron emission. SSC with target photons coming from electron synchrotron emission is the dominant (leptonic) mechanism to produce the observed hard X-rays and low energy  $\gamma$ -rays, while neutral pion decays resulting from  $pp$  inelastic collisions is the dominant hadronic process to produce the high energy  $\gamma$ -rays, and neutral pion decays resulting from photo-meson interaction ( $p\gamma$ ) the dominant one to produce the very high energy (VHE)  $\gamma$ -rays. Interestingly, in the case of the microquasars Cyg X1 and Cyg X3, KGV15 have also found that the core model could reproduce the full observed SED including the low and high energy branches.<sup>6</sup>

<sup>6</sup> We should remark that the observed emission at low energies (radio to optical) from the core regions in the case of Cen A and M87 is fitted by the core model described here only if we assume that the minimum electron energy injected in the acceleration region is a few times the particle rest mass. If one considers

#### 4.5. Conclusions

- We have presented a reconnection acceleration model in the core region around the BH of the low luminous radio galaxies Cen A, Per A, M87 and IC 310 and showed that it is able to reproduce very well their SEDs, from radio to gamma-rays up to TeV energies.
- This is complementary to a recent study where we have performed similar analysis for the galactic black hole binaries, i.e., the microquasars Cyg X1 and X3 (Khiali et al. 2015). Together, these two works strengthen the conclusions of the previous works of Kadowaki et al. (2015) and Singh et al. (2015) in favour of a core emission specially for the observed gamma-ray radiation of microquasars and LLAGNs (which belong to the so called fundamental plane of BH activity).
- Magnetic reconnection acceleration seems to provide a better efficiency in regions where magnetic activity is dominant in comparison with diffusive shock acceleration as the cores of LLAGNs. Particles can gain energy up to a few times  $\sim 100$  TeV due to magnetic reconnection acceleration.
- The observed TeV  $\gamma$ -ray emission may be originated in these cores via neutral pion decays in hadronic processes.
- The fast magnetic reconnection acceleration model occurring in the core of these sources can naturally explain the observed short time variability, specially of the high energy  $\gamma$ -ray.

Finally, we note that it is possible that a neutrino spectrum may be also produced in the nuclear region of LLAGNs considering the same model here investigated, as due to charged pion decays via  $pp$  and  $p\gamma$  interactions. In a concomitant work, this possibility has been investigated to explain the recently observed extragalactic neutrino flux by the IceCube experiment (Khiali & de Gouveia Dal Pino 2015).

#### Acknowledgements

This work has been partially supported by grants from the Brazilian agencies FAPESP (2013/10559-5), CNPq (306598/2009-4), and CAPES. We also acknowledge useful discussions with Paola Grandi in the selection of data for the construction of the SEDs.

#### References

Abdo, A. A., et al. 2009a, *ApJ*, 699, 31  
 Abdo, A. A., et al. 2009b, *ApJ*, 700, 597  
 Abdo, A. A., et al. 2009c, *ApJ*, 707, 55  
 Abdo, A. A., et al. 2010, *ApJ*, 719, 1433  
 Abraham, J., et al. 2007, *Science*, 318, 938  
 Abramowski, A., et al. 2012, *ApJ*, 746, 151  
 Ackermann, M., et al. 2012, *ApJS*, 203, 4

Ade, P. A. R. et al. 2011, *A&A*, 536, 7  
 Aharonian, F. A., Akhperjanian, A., Beilicke, M., et al. 2003, *A&A*, 403, L1  
 Aharonian, F. A., et al. 2006, *Science*, 314, 1424  
 Aharonian, F. A., et al. 2009, *ApJL*, 695, L40  
 Ajello, M., et al. 2009, *ApJ*, 690, 367  
 Aleksić, J., et al. *ApJ*, 723, L207  
 Aleksić, J., et al. *ApJ*, 710, 634  
 Aleksić, J., et al. *A&A*, 539, L2  
 Aleksić, J., et al. *A&A*, 541, 99  
 Aleksić, J., Antonelli, L. A., et al. 2014a, *A&A*, 563, A91  
 Aleksić, J., Ansoldi, S., Antonelli, L. A., et al. 2014b, *A&A*, 564, AA5  
 Aleksić, J., Ansoldi, S., Antonelli, L. A., et al. 2014c, *Science*, 346, 1080  
 Asada, K., Kamenou, S., Shen, Z. Q. et al. 2006, *Publ. Astron. Soc. Japan*, 58, 261  
 Barkov, M. V., Bosch-Ramon, V., & Aharonian, F. A. 2012, *ApJ*, 755, 170  
 Becker, R. H., White, R. L., & Edwards, A. L. 1991, *APJS*, 75, 1  
 Bernardi, M., Alonso, M. V., da Costa, L. N., et al. 2002, *AJ*, 123, 2990  
 Biretta, J. A., Stern, C. P., & Harris, D. E. 1991, *AJ*, 101, 1632  
 Biretta, J. A., Sparks, W. B., & Macchetto, F. 1999, *ApJ*, 520, 621  
 Brown, A. M. & Adams, J. 2011, *MNRAS*, 413, 2785  
 Buttiglione, S., Capetti, A., Celotti, A., et al. 2010, *A&A*, 509, A6  
 Canning, R. E. A., Fabian, A. C., Johnstone, R. M., et al. 2010, *MNRAS*, 405, 115  
 Cerutti, B., Dubus, G., Malzac, J., et al. 2011, *A&A* 529, A120  
 Cerutti, B., Werner, G. R., Uzdensky, D. A., Begelman, M. C. 2013, *ApJ*, 770, 147C  
 Cerutti, B., Werner, G. R., Uzdensky, D. A., Begelman, M. C. 2014, *ApJ*, 782, 104C  
 Chiaberge, M., Capetti, A., & Celotti, A. 1999, *A&A*, 349, 77  
 Condon, J. J., Cotton, W. D., & Broderick, J. J. 2002, *AJ*, 124, 675  
 de Gouveia Dal Pino, E. M. & Lazarian, A. 2005, *Astronomy and Astrophysics*, 441, 845  
 de Gouveia Dal Pino, E. M., Piovezan, P. P. & Kadowaki, L. H. S. 2010a, *Astronomy and Astrophysics*, 518, A5  
 de Gouveia Dal Pino, E. M., Kowal, G., Kadowaki, L. H. S., Piovezan, P. P., & Lazarian, A. 2010b, *International Journal of Modern Physics D*, 19, 729  
 de Gouveia Dal Pino, E. M., Kowal, G., Lazarian, A. 2014, 8th International Conference of Numerical Modeling of Space Plasma Flows (ASTRONUM 2013), 488, 8, arXiv1401.4941D  
 de Gouveia Dal Pino, E. M., & Kowal, G. 2015, in *Magnetic Fields in Diffuse Media* (eds. A. Lazarian, E. M. de Gouveia Dal Pino, C. Melioli), *Astrophysics and Space Science Library*, 407, 373  
 Despringre, V., Fraix-Burnet, D., & Davoust, E. 1996, *A&A*, 309, 375  
 Dexter, J., McKinney, J. C., Markoff, S., & Tchekhovskoy, A. 2014, *MNRAS*, 440, 218  
 Douglas, J. N., Bash, F. N., Bozayan, F. A., Torrence, G. W., & Wolfe, C. 1996, *AJ*, 111, 1945  
 Drake, J. F., Swisdak, M., Che, H. and Shay, M. A. 2006, *Nature*, 443, 553D  
 Drake, J. F., Opher, M., Swisdak, M. and Chamoun, J. N. 2010, *ApJ*, 709, 963D  
 Drury, L. 2012, *MNRAS*, 422, 2474D  
 Dunn, R. J. H., Allen, S. W., Taylor, G. B., et al. 2010, *MNRAS*, 404, 180  
 Eyink, G. L., Lazarian, A., & Vishniac, E. T. 2011, *ApJ*, 743, 51  
 Falceta-Gonçalves, D., Caproni, A., Abraham, Z., Teixeira, D. M., & de Gouveia Dal Pino, E. M. 2010, *ApJL*, 713, L74  
 Gebhardt, K. & Thomas, J. 2009, *ApJ*, 700, 1690  
 Georgopoulos, M., Perlman, E. S., & Kazanas, D., 2005, *ApJL*, 634, 33  
 Giannios, D., Uzdensky, D. A. & Begelman, M. C. 2010, *MNRAS*, 402, 1649  
 Ginzburg, V. L., & Syrovatskii, S. I. 1995, *ARA&A*, 3, 297  
 Graham, J. A. 1978, *PASP*, 90, 237  
 Hardcastle, M. J., Worrall, D. M., Kraft, R. P., Forman, W. R., Jones, C., & Murray, S. S. 2003, *ApJ*, 593, 169  
 Hardcastle, M. J., Cheung, C. C., Feain, I. J., & Stawarz, L. 2009, *MNRAS*, 393, 1041  
 Harmon, B. A., Wilson, C. A., Fishman, G. J., et al. 2004, *ApJS*, 154, 585  
 Hartman, R. C., et al. 1999, *ApJS*, 123, 79  
 Hawarden, T. G., Sandell, G., Matthews, H. E., et al. 1993, *MNRAS*, 260, 844  
 Ho, L. C., Filippenko, A. V., & Sargent, W. L. W. 1997, *ApJS*, 112, 315



- Istomin, Y. N., & Sol, H. 2009, *Astrophys. Space Sci.*, 321, 57
- Johnstone, R. M., & Fabian, A. C. 1995, *MNRAS*, 273, 625
- Kachelriess, M., Ostapchenko, S., & Tomas, R. 2009b, *Int. J. Mod. Phys. D* 18, 1591
- Kachelriess, M., Ostapchenko, S., & Tomas, R. 2010, arXiv: 1002.4874
- Kadler, M., Eisenacher, D., Ros, E., et al. 2012, *A&A*, 538, L1
- Kadowaki, L. H. S., de Gouveia Dal Pino, E. M., & Singh, C. B. 2015, *ApJ*, 802, 113 (KGS15)
- Kalberla, P. M. W., McClure-Griffiths, N. M., Pisano, D. J., et al. 2010, *A&A*, 521, A17
- Kellermann, K. I., Lister, M. L., Homan, D. C., et al. 2004, *ApJ*, 609, 539
- Khiali, B., de Gouveia Dal Pino, E. M. & del Valle, M. V. 2015, *MNRAS*, 449, 34 (KGV15)
- Khiali, B., & de Gouveia Dal Pino, E. M. 2015, arXiv:1506.01063
- Kinzer, R. L., et al. 1995, *ApJ*, 449, 105
- Koide, S., Shibata, K., Kudoh, T., & Meier, D. L. 2002, *Science*, 295, 1688
- Kowal, G., Lazarian, A., Vishniac, E. T., Otmianowska-Mazur, K. 2009, *ApJ*, 700, 63
- Kowal, G., de Gouveia Dal Pino, E. M., Lazarian, A. 2011, *The Astrophysical Journal*, 735, 102
- Kowal, G., de Gouveia Dal Pino, E. M., Lazarian, A. 2012, *Physical Review Letters*, 108, 241102
- Lazarian, A., & Vishniac, E. T. 1999, *The Astrophysical Journal*, 517, 700
- Lazarian, A., Vlahos, L., Kowal, G., Yan, H., Beresnyak, A. & de Gouveia Dal Pino, E. M. 2012, *Space Science Reviews*, 173, 557
- Lazarian, A., Takamoto, M., de Gouveia Dal Pino, E., Cho, J. 2015, in press.
- Lenain, J. P., Boisson, C., Sol, H. & Katarzynski, K. 2008 *A&A*, 478, 111
- Levinson, A., 2000, *Phys. Rev. Lett.*, 85, 912
- Lieu, R., Mittaz, J. P. D., Bowyer, S., et al. 1996, *ApJ*, 458, L5
- Lin, R. P., & Hudson, H. S. 1971, *SoPh*, 17, 412
- Lister, M. L., Aller, H. D., Aller, M. F. et al. 2009, *AJ*, 137, 3718
- Liu, F. K. and Chen, X. 2007 *ApJ*, 671, 1272
- Liu, B. F., Mineshige, S., & Ohsuga, K. 2003, *ApJ*, 587, 571
- MacDonald, D. A., Thorne, K. S., Zhang, X.-H., & Price, R. H. 1986, *Black Holes: The Membrane Paradigm*, 121
- Marconi, A., Pastorini, G., Pacini, F., Axon, D. J., Capetti, A., Macchetto, D., Koekemoer, A. M., & Schreier, E. J. 2006, *A&A*, 448, 921
- Markowitz, A., et al. 2007, *ApJ*, 665, 209
- Mariotti, M. 2010, *ATel*, 2510
- Merloni, A., Heinz, S., & di Matteo, T. 2003, *MNRAS*, 345, 1057
- Mirabel, I. F., Laurent, O., Sanders, D. B., et al. 1999, *A&A*, 341, 667
- Morganti, R., Oosterloo, T., Struve, C., & Saripalli, L. 2008, *A&A*, 485, L5
- Nagar, N. M., Falcke, H., & Wilson, A. S. 2005, *A&A*, 435, 521
- Neronov, A., & Aharonian, F. A. 2007, *ApJ*, 671, 85
- Neronov, A., Demikoz, D., & Vovk, I. 2010, *A&A*, 519, L6
- Neumayer, N., Cappellari, M., Reunanen, J., Rix, H. W., van der Werf, P. P., de Zeeuw, P. T., & Davies, R. I. 2007, *ApJ*, 671, 1329
- Oishi, J. S., Mac Low, M.-M., Collins, D. C., & Tamura, M. 2015, *ApJL*, 806, L12
- Pedlar, A., Ghataure, H. S. et al. 1990, *MNRAS*, 246, 477
- Perlman, E. S., Sparks, W. B., Radomski, J., et al. 2001, *ApJ*, 561, L51
- Priest, E. R. 2001, *Earth Planets Space*, 53, 483
- Reimer, A., Protheroe, R. J. & Donea, A. C. 2004, *A&A*, 419, 89
- Rejkuba, M. 2004, *A&A*, 413, 903
- Retinò, A., Sundkvist, D., Vaivads, A., et al. 2007, *Nature Physics*, 3, 236
- Reynoso, M. M., Medina, M. C. and Romero, G. E. 2011, *A&A* 531, A30, 201
- Romero, G. E., Christiansen, H. R., Orellana, M. 2005, *apj* 632,1093, 2005
- Ryter, C. E. 1996, *Ap&SS*, 236, 285
- Sahu, S., Zhang, B., & Fraija, N. 2012, *Physical Review Letters*, 85, 043012
- Sato, K., Furusho, T., Yamasaki, N. Y., et al. 2005, *PASJ*, 57, 743
- Shi, Y., Rieke, G. H., Hines, D. C., Gordon, K. D., & Egami, E. 2007, *ApJ*, 655, 781
- Singh, C. B., de Gouveia Dal Pino, E. M. & Kadowaki, L. H. S. 2015, *ApJ*, 799, L20
- Sol, H., Zech, A., Boisson, C., et al. 2013, *Astroparticle Physics*, 43, 215
- Soldi, S., Beckmann, V., Baumgartner, W. H., et al. 2014, *A&A*, 563, A57
- Sparks, W. B., Biretta, J. A., & Macchetto, F. 1996, *ApJ*, 473, 254
- Spruit, H. C. 1988, *A&A*, 194, 319
- Sreekumar, P., Bertsch, D. L., Hartman, R. C., Nolan, P. L., & Thompson, D. J. 1999, *Astropart. Phys.*, 11, 221
- Stawarz, L., Siemiginowska, A., Ostrowski, M., & Sikora, M. 2005, *ApJ*, 626, 120
- Stawarz, L., Kneiske, T. M., & Kataoka, J. 2006, *ApJ*, 637, 693
- Steinle, H., et al. 1998, *A&A*, 330, 97
- Tan, J. C., Beuther, H., Walter, F., & Blackman, E. G. 2008, *ApJ*, 689, 775
- Tavecchio F., Ghisellini G., 2008, *MNRAS*, 385, L98
- Tingay S. J., et al. 1998, *AJ*, 115, 960
- Torresi, E. 2012, arXiv:1205.1691
- Vermeulen, R. C., Readhead, A. C. S., Backer, D. C. 1994, *ApJ*, 430, L41
- Vincent, S., 2014, arXiv:1411.1957
- Walker R. C., Romney J. D., Benson J. M. 1994, *ApJ*, 430, L45
- White, R. L., & Becker, R. H. 1992, *APJS*, 79, 331
- Wilman R. J., Edge A. C., Johnstone R. M. 2005, *MNRAS*, 359, 755
- Wilson-Hodge, C. A., Case, G. L., Cherry, M. L., et al. 2012, *ApJS*, 201, 33
- Yamada, M., Jongsoo, Y., Jonathan J. A., Hantao, J., Russell M. K. Zenitani, S., Hesse, M. & Klimas, A. 2009, *ApJ*, 696, 1385Z